J|A|C|S COMMUNICATIONS

Published on Web 02/17/2010

Anisotropic Strain-Induced Curvature in Type-II CdSe/CdTe Nanorod Heterostructures

Hunter McDaniel, Jian-Min Zuo, and Moonsub Shim*

Department of Materials Science and Engineering and Frederic Seitz Materials Research Laboratory, University of Illinois at Urbana-Champaign, Urbana, Illinois 61801

Received December 9, 2009; E-mail: mshim@illinois.edu

Semiconductor nanocrystal heterostructures (NCHs) are adding new dimensions to the ways in which unique size-tunable electronic and optical properties of nanocrystals can be engineered. For example, the ability to bring together various semiconductors with different energy band offsets has allowed NCHs to improve fluorescence quantum yields,[1] eliminate photoluminescence blinking,[2] and overcome the fast Auger recombination problem in lasing.[3] Currently, there is an increasing interest in NCHs that can promote photoinduced charge separation.[4−6] A shell-thickness-dependent transition from type-I to type-II band offset has been demonstrated in ZnSe/CdSe core/shell NCHs.[5] Such a transition can also be induced by lattice strain in core/shell NCHs.[6] In addition to these approaches to tuning the relative band offsets, nanorod (NR)-based[7−11] and nanowire-based[12] heterostructures with inherent anisotropy can provide directionality in charge separation, which is necessary for many energy applications. Here we report anisotropic strain in CdSe NRs driven by the growth of lattice-mismatched CdTe. Atomic resolution *Z*-contrast scanning transmission electron microscopy (STEM) in addition to high-resolution TEM (HRTEM) was used to characterize the interfaces of these NR heterostructures (NRHs), revealing strain-induced curvature. Linear barbell-shaped NRHs were also synthesized and compared.

Curved CdSe/CdTe NRHs were synthesized by direct slow addition of trioctylphosphine telluride (TOPTe) to the CdSe NR reaction mixture followed by a brief (∼5 min) aging at 300 °C, similar to the methods of Koo et al.[13] and Kumar et al.[10] The NRHs shown in Figure 1 were synthesized using seed CdSe NRs with average length and diameter of 23.7 and 4.2 nm, respectively [see the Supporting Information (SI)]. Growth of CdTe increased the average length by ∼36% and the average diameter in the center by a few monolayers. The diameter of the tips was on average ∼88% larger than the initial seed NR diameter. HRTEM images indicate that the lattice constant in the central part of the NRHs is the same as that of the CdSe seeds, whereas the tips show on average the ∼7% expansion expected of the larger CdTe lattice.

Under the synthesis conditions employed, mostly tip growth was expected and observed here, but significant growth of CdTe beyond the tips to the sides of the seed NRs also occurred. There was also a striking and unexpected curvature in these NRHs. In fact, a careful examination of TEM images in previous reports of CdSe/CdTe NRHs shows that similar bends are sometimes present (e.g., see Figure 1B of ref 13). In our case as well as in previous reports,[8−10] the seed CdSe NRs did not exhibit any noticeable curvature (see the SI). The HRTEM image in Figure 1B indicates that this curvature arises from an actual deflection in the lattice planes. As expected, control experiments (not shown) indicated that heating CdSe seed NRs to 300 °C for a prolonged period of time (1 h) in the absence of the Te reagent did not lead to the observed curvature. In view of the substantial mismatch between CdSe and CdTe, lattice strain is expected in this system. However, the lattice expanded

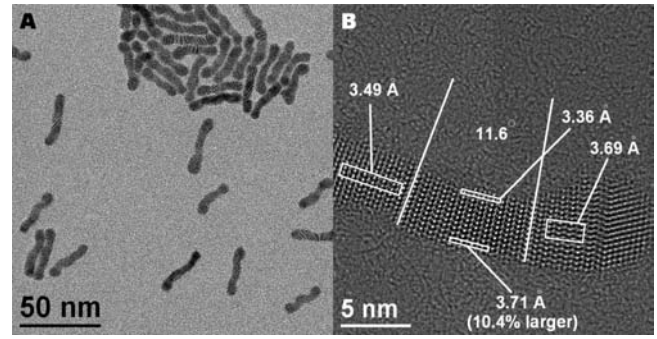

Figure 1. TEM images of highly strained CdSe/CdTe NRHs at (A) low and (B) high resolution. In (B), the lattice is bent by 11.6° over an ∼8.7 nm arc distance, corresponding to a 41 nm inner radius of curvature. The (0002) lattice spacing for the boxed regions are indicated. The lattice expands by 10.4% from the inner to the outer part of the curvature. While the outer part is similar to the CdTe lattice constant, the inner part is ∼4% smaller than CdSe lattice parameter.

from the inner to the outer part of the curved region much more than expected from the bulk lattice parameters. The expected (0002) lattice spacing (d_{0002}) difference between CdSe and CdTe is 6.6% (with respect to the smaller CdSe d_{0002}). The NRH in Figure 1B exhibits an expansion of 10.4% from the inner to the outer part of the curvature. We have observed lattice expansion as large as 13% (see the SI).

For the nonalloyed CdSe/CdTe NRHs, one would expect the smaller CdSe lattice to be under tension and the larger CdTe lattice to be under compression. Alloying is not expected here since Se/Te interdiffusion in NRHs is insignificant at our growth temperature and time.[13] On the outer part of the curvature of the NRH Figure 1B, $d_{0002} = 3.71$ Å, which is only ∼1% smaller than the expected lattice spacing for CdTe. However, the d_{0002} of the inner part of the curvature is 3.36 Å, ∼4% *smaller* than that of CdSe. Since alloying between CdSe and CdTe would always lead to lattice spacing larger than that of CdSe, alloying, again, is not expected and cannot explain these results. Control experiments in which both the seed CdSe NRs and the resulting CdSe/CdTe NRHs were imaged together further verified that the small lattice spacing observed here is indeed smaller than in the original CdSe NRs (see the SI).

To better understand the cause of this unusual lattice compression and the associated curvature, we carried out atomic-resolution *Z*-contrast imaging using aberration-corrected STEM. When a wurtzite crystal is viewed along the $[11\bar{2}0]$ zone axis, the atomic positions of all of the cations (and anions) line up vertically, and therefore, the integrated composition of each column of ions is projected in the STEM image. The atomic number difference allows easy identification of cations and anions. A column of higher atomic number Cd cations ($Z = 48$) scatters a beam of electrons more

10.1021/ja910233a

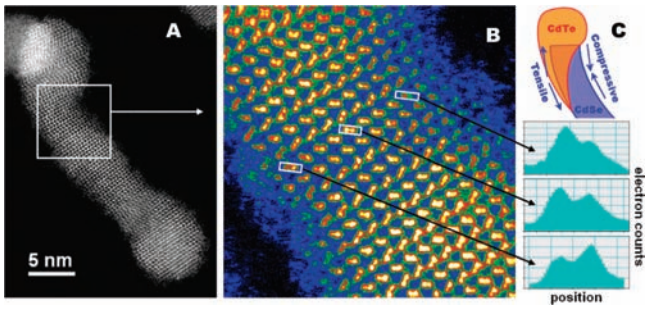

Figure 2. (A) Low- and (B) high-resolution STEM images of a curved NRH. When imaged along the [11$\bar{2}$0] zone axis, cation/anion columns can be resolved, revealing a *Z*-contrast inversion near the center of the rod. *Z*-contrast profiles of anion/cation pair columns at the indicated points are shown to the right of (B). (C) Schematic outlining the regions expected to be CdSe and CdTe on the basis of the *Z*-contrast image and observed lattice expansion.

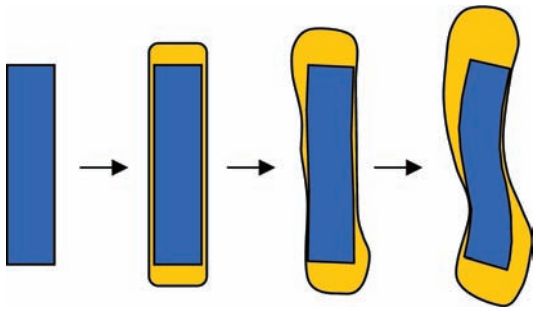

Figure 3. Schematic of a possible growth mechanism for the curved NRHs. The first few monomlayers of CdTe are deposited nearly uniformly, with the exception of faster growth at the tips. As CdTe grows in size, strain builds up, causing island formation and inducing curvature. Tips with faster growth rates are more likely to form the initial CdTe islands, which continue to grow. Occasionally, CdTe islands can also form near the center, causing apparent multiple bends.

strongly than a column of Se anions ($Z = 34$) and thus appears brighter in the *Z*-contrast STEM image. CdTe has the opposite contrast, since the Te anions have the higher atomic number ($Z = 52$). The profiles shown to the right of Figure 2B demonstrate that in these NRHs, such a cation−anion *Z*-contrast inversion is easily observed from the inner to the outer part of the curved region. That is, CdTe not only deposits at the tips but also extends out partly alongside the NR seeds, specifically along the outside of the curvature. Deposition of CdTe imperfectly at the tips of the CdSe NRs (i.e., partly on the sides as well) imposes tension parallel and perpendicular to the (0001) interface at the tip. In the absence of dislocations or other strain-relieving defects, a substantial *compressive strain* builds up in the location directly opposite the side where CdTe is partially deposited, leading to the observed curvature.

The emerging picture of how the curved NRHs form is shown schematically in Figure 3. The first few monolayers of CdTe are deposited uniformly on the seed CdSe NRs. Even at this stage, tip growth is faster, as verified by TEM (Figure S6 in the SI). As CdTe continues to grow, the lattice mismatch causes strain to build up and in turn leads to island growth analogous to the well-known Stranski−Krastinow growth mechanism in thin-film heteroepitaxy. Since the growth rate is faster at the tips, the initial island formation is more likely to occur there. Hence, the majority of the bends are observed near the tips. In addition to the transition from uniform deposition to island growth, the NR geometry allows a unique phenomenon to be observed here. That is, NRHs minimize their strain energy by bending. Because of the small diameters of the NRs, bending may be energetically more favorable than introducing

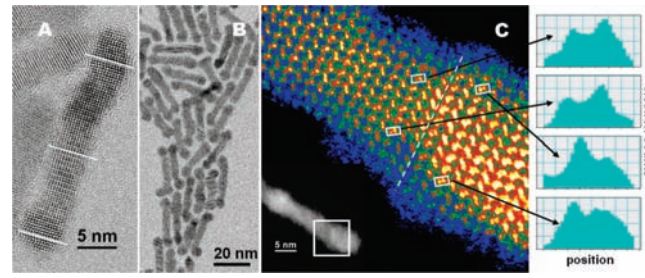

Figure 4. (A) High- and (B) low-resolution TEM images of linear barbell NRHs. Parallel lines drawn along the (0002) planes demonstrate the absence of strain-induced curvature. (C) High- and (inset) low-resolution STEM images. The boxed region of the inset is magnified in the main panel. Contrast profiles of anion/cation pair columns at the four points indicated reveal a *Z*-contrast inversion. The left side of the dashed line in (C) is CdSe, while the right side is CdTe.

strain-relieving dislocations. We have not observed any dislocations in HRTEM images of these curved NRHs. The curvature further hinders CdTe growth on the sides opposite those where the initial CdTe islands have formed, as a result of the even larger lattice mismatch caused by the unusual compression of the seed CdSe NRs. Thus, the bending of the seed NRs enhances additional CdTe deposition onto the existing CdTe on the outside part of the curvature relative to the inner part, leading to positive feedback for curvature formation. Occasional bends and bumps can also be observed near the middle parts of the seed NRs (Figure 1A). These cases are usually accompanied by curvature near the tips. Additional CdTe island formation may occur near the middle of the seed NR, leading to NRHs with multiple bends.

For comparison, we also synthesized CdSe/CdTe NRHs that do not exhibit curvature. Linear barbell structures as shown in Figure 4 were obtained by lower-temperature (250 °C) injection of the Te reagent. The fact that the reaction temperature was the only parameter varied here indicates that the differentiation of tip and side growth can easily be obtained, with the threshold for side nucleation of CdTe being between 250 and 300 °C. The linear NRHs exhibited an average length increase of ∼58%, whereas the average center width increase was negligible (<1%). The inset of Figure 4A shows an HRTEM image indicating that these linear barbell-shaped NRHs do not exhibit the anisotropic strain-induced curvature/bends. The lines identifying the lattice fringe direction near the tips are parallel to each other and to the analogous line near the center of the NRH. The lack of curvature is expected here, since side growth of CdTe, which is necessary to induce strain parallel to the rod axis, is suppressed. High-resolution STEM imaging (Figure 4C) showed a very sharp CdSe/CdTe interface with an upper limit of 3−4 atomic steps, as verified by the observed inversion in the *Z*-contrast profile line scans (see the SI). Notably, the actual interface should be sharper, since the contrast seen in the STEM image is a projection of integrated compositions along a column of ions parallel to the zone axis. We suspect that the interface in the curved structure is similarly sharp. However, since CdTe partially overcoats the seed NR in this case, the cation−anion *Z*-contrast image gives the average of CdSe and CdTe near the center of the curve region, as indicated by the similar intensities shown in the middle *Z*-contrast profile to the right of Figure 2B.

Finally, we comment on the possible effects of strain on the band offsets and therefore the ability of these NRHs to separate charges. In the linear barbell-shaped NRHs, the expected type-II band offset based on flat band potentials would be modified by strain in the following manner. The conduction band edge energy of CdSe would be lowered as a result of tension, whereas that of CdTe would be increased because of compression. The net effect would be an

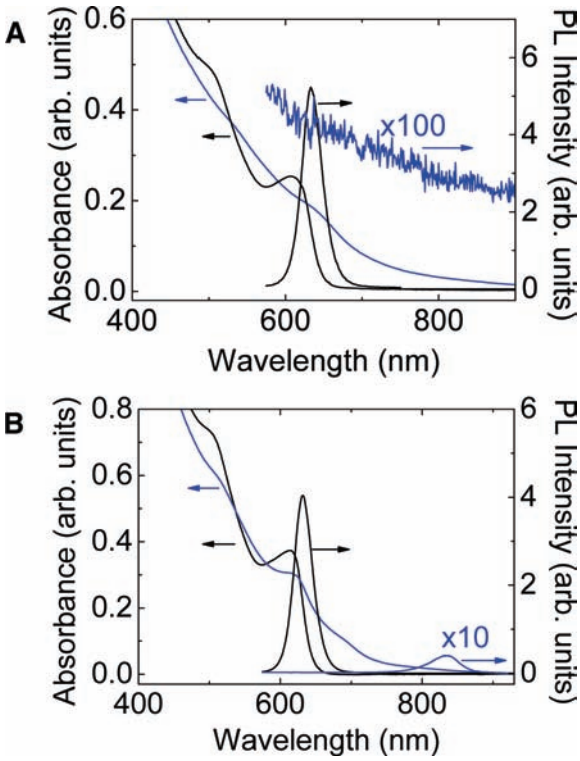

Figure 5. Absorption and PL spectra of (A) curved and (B) linear CdSe/CdTe NRHs (blue). Corresponding spectra of the seed CdSe NRs (black) are also shown. The PL spectra have been normalized to the absorbance at the excitation wavelength.

increase in the band offset, or enhanced type-II character, as has been shown in the core/shell analogue.[6] However, in the presence of the curvature, where part of the CdSe is under compression, selective localization of electrons may be possible because of the increasing conduction band energy away from the heterointerface in the CdSe region. Such effects may be manifested in their optical properties, especially in their photoluminescence (PL). Figure 5 shows the absorption and PL spectra of curved and linear NRHs along with the spectra of the corresponding seed CdSe NRs. Both types of NRHs exhibited the expected absorption tail at photon energies below the CdTe band-edge transition. These absorption tails arise from the charge-transfer excitations of the type-II heterostructures. We also observed the corresponding large Stokes-shifted PL for the linear barbell structures (at ~2 orders of magnitude lower efficiency than for the initial seed CdSe NRs). However, the curved NRHs did not exhibit detectable PL at room temperature. We suspect that carrier trapping, especially the hole, on the surface is the dominating factor in the curved NRHs, since the larger portion of the heterointerface is only about two monolayers away from the surface. Notably, for the linear barbell structures, previous reports have shown both complete quenching[9] and weak but non-negligible[10] Stokes-shifted PL (as we do here). We suspect that these apparent contradictory results arise from the differences in the synthetic procedures employed. In ref 9, an additional step was taken wherein the seed NRs were precipitated and redissolved before the CdTe growth step was carried out. On the other hand, a one-pot synthesis in which the seed CdSe NRs were never taken out of the N_2 atmosphere of the reaction flask was utilized in ref 10. The seed CdSe NRs of the latter one-pot synthesis approach are more likely to start with higher PL yields, and therefore, the resulting NRHs may also be expected to exhibit higher PL quantum yields. The weak Stokes-shifted PL of the linear barbell structures observed here is consistent with these expectations.

We have presented atomic-resolution imaging of both linear and curved NRHs. In the absence of strain-relieving defects, surprisingly large compressive strain of ~4% leading to an overall axial deflection can be induced in the seed CdSe NRs when the larger-lattice CdTe is deposited on both the tips and the sides of the seeds. While both curved and linear structures are expected to exhibit sharp interfaces, only the linear NRHs have CdTe localized at the tips. Because of this topological difference, only the linear barbell structures exhibit weak, large Stokes-shifted PL at room temperature. Quenching of PL in the curved NRHs may be associated with charge trapping at the surface in close proximity to the heterointerface where charge separation occurs. Charge-transfer absorption features of type-II band-offset materials, on the other hand, are observed in both types of NRHs. In combination with the ability to control the location where CdTe is deposited on the seed CdSe NRs, the strain effects observed here may provide new approaches to directing the separation of photogenerated carriers, which may facilitate incorporation of NRHs in various energy applications.

Acknowledgment. This material is based upon work supported by the ACS PRF under Grant 46443-AC10. TEM was carried out in the Center for Microanalysis of Materials, University of Illinois, which is partially supported by the U.S. Department of Energy under Grant DEFG02-91-ER45439.

Supporting Information Available: Experimental procedures, additional TEM and STEM images, size distributions, and XRD and EDS data. This material is available free of charge via the Internet at http://pubs.acs.org.

References

(1) Hines, M. A.; Guyot-Sionnest, P. *J. Phys. Chem.* **1996**, *100*, 468.
(2) Wang, X.; Ren, X.; Kahen, K.; Hahn, M. A.; Rajeswaran, M.; Maccagnano-Zacher, S.; Silcox, J.; Cragg, G. E.; Efros, A. L.; Krauss, T. D. *Nature* **2009**, *459*, 686.
(3) Klimov, V. I.; Ivanov, S. A.; Nanda, J.; Achermann, M.; Bezel, I.; McGuire, J. A.; Piryantinski, A. *Nature* **2007**, *447*, 441.
(4) Kim, S.; Fisher, B. R.; Eisler, H.-J.; Bawendi, M. *J. Am. Chem. Soc.* **2003**, *125*, 11466.
(5) Balet, L. P.; Ivanov, S. A.; Piryatinski, A.; Achermann, M.; Klimov, V. I. *Nano Lett.* **2004**, *4*, 1485.
(6) Smith, A. M.; Mohs, A. M.; Nie, S. *Nat. Nanotechnol.* **2009**, *4*, 56.
(7) Milliron, D. J.; Hughes, S. M.; Cui, Y.; Manna, L.; Li, J. B.; Wang, L.-W.; Alivisatos, A. P. *Nature* **2004**, *430*, 190.
(8) Shieh, F.; Saunders, A. E.; Korgel, B. A. *J. Phys. Chem. B* **2005**, *109*, 8538.
(9) Halpert, J. E.; Porter, V. J.; Zimmer, J. P.; Bawendi, M. G. *J. Am. Chem. Soc.* **2006**, *128*, 12590.
(10) Kumar, S.; Jones, M.; Shun, S. L.; Scholes, G. D. *Small* **2007**, *3*, 1633.
(11) McDaniel, H.; Shim, M. *ACS Nano* **2009**, *3*, 434.
(12) Goebl, J. A.; Black, R. W.; Puthussery, J.; Giblin, J.; Kosel, T. H.; Kuno, M. *J. Am. Chem. Soc.* **2008**, *130*, 14822.
(13) Koo, B.; Korgel, B. A. *Nano Lett.* **2008**, *8*, 2490.

JA910233A